REPORT DOCUMENTATION PAGE

Form Approved
OMB No. 0704-0188

1. REPORT DATE *(DD-MM-YYYY)*
15-06-2010

REPRINT

4. TITLE AND SUBTITLE
Tracking Nonradial Motions and Azimuthal Expansions of Interplanetary CMEs with the Solar Mass Ejection Imager

5a. CONTRACT NUMBER

5b. GRANT NUMBER

5c. PROGRAM ELEMENT NUMBER
62601F

6. AUTHOR(S)
Kahler, Stephen and David Webb*

5d. PROJECT NUMBER
5021

5e. TASK NUMBER
RD

5f. WORK UNIT NUMBER
A1

7. PERFORMING ORGANIZATION NAME(S) AND ADDRESS(ES)
Air Force Research Laboratory/RVBXS
29 Randolph Road
Hanscom AFB MA 01731-3010

8. PERFORMING ORGANIZATION REPORT NUMBER
AFRL-RV-HA-TR-2010-1049

9. SPONSORING / MONITORING AGENCY NAME(S) AND ADDRESS(ES)

10. SPONSOR/MONITOR'S ACRONYM(S)
AFRL/RVBXS

11. SPONSOR/MONITOR'S REPORT NUMBER(S)

12. DISTRIBUTION / AVAILABILITY STATEMENT
Approved for Public Release; Distribution Unlimited.

*Institute for Scientific Research, Boston College, Chestnut Hill, MA

13. SUPPLEMENTARY NOTES
REPRINTED FROM: CP1216, 12th International Solar Wind Conference, pp 408-411, 2010

14. ABSTRACT

Abstract. The trajectories of interplanetary CMEs (ICMEs) are modified by their interactions with solar wind streams. These interactions can result in non-radial deflections of ICME trajectories and changes to their rates of azimuthal expansion. The Solar Mass Ejection Imager (SMEI), launched earlier in 2003 January, has provided heliospheric images of several hundred ICMEs during the declining portion of solar cycle 23. We selected three SMEI ICMEs, each traversing a range of solar elongation angles $\varepsilon > 20°$, and measured the time changes of their leading-edge profiles plotted against position angle, PA. The parabolic fits to those profiles yielded the propagation directions of the ICMEs as well as their leading-edge curvatures and time profiles. The selected ICMEs were associated with LASCO CMEs, so we tracked the PA variations in their propagation over 1 to 3-day periods. We found good fits for two of the ICMEs, but one yielded generally poor fits.

15. SUBJECT TERMS
Coronal mass ejections Solar physics Heliospheric imaging CMEs

16. SECURITY CLASSIFICATION OF:	17. LIMITATION OF ABSTRACT	18. NUMBER OF PAGES	19a. NAME OF RESPONSIBLE PERSON
a. REPORT UNCLAS		4	Janet C. Johnston
			19b. TELEPHONE NUMBER *(include area code)* 781-377-2138

Tracking Nonradial Motions and Azimuthal Expansions of Interplanetary CMEs with the Solar Mass Ejection Imager

Stephen Kahler* and David Webb†

*Space Vehicles Directorate, AFRL/RVBXS, 29 Randolph Rd, Hanscom AFB, MA USA
†Institute for Scientific Research, Boston College, Boston MA USA

Abstract. The trajectories of interplanetary CMEs (ICMEs) are modified by their interactions with solar wind streams. These interactions can result in non-radial deflections of ICME trajectories and changes to their rates of azimuthal expansion. The Solar Mass Ejection Imager (SMEI), launched earlier in 2003 January, has provided heliospheric images of several hundred ICMEs during the declining portion of solar cycle 23. We selected three SMEI ICMEs, each traversing a range of solar elongation angles $\varepsilon > 20°$, and measured the time changes of their leading-edge profiles plotted against position angle, PA. The parabolic fits to those profiles yielded the propagation directions of the ICMEs as well as their leading-edge curvatures and time profiles. The selected ICMEs were associated with LASCO CMEs, so we tracked the PA variations in their propagation over 1 to 3-day periods. We found good fits for two of the ICMEs, but one yielded generally poor fits.

Keywords: coronal mass ejection
PACS: 96.60ph, 96.50Uv

THE SOLAR MASS EJECTION IMAGER (SMEI)

The SMEI instrument is the first all-sky imager in orbit and was launched aboard the Coriolis spacecraft in 2003 January. SMEI is in an 840 km circular, Sun-synchronous orbit along the Earth's terminator. It consists of three cameras that map nearly the entire sky in white light every 102 minutes [5]. The mission goal is to demonstrate the feasibility of detecting interplanetary coronal mass ejections (ICMEs) against the much brighter background sky. The basic SMEI goals and requirements are [12]:

- Fly a proof-of-concept Air Force experiment
- Track ICMEs from Sun to Earth
- Provide an all-sky view, updated every orbit
- Detect signal at 1% of background (zodiacal light and stars)

The SMEI uses 3 baffled CCD cameras, each of which observes a $60° \times 3°$ strip of sky with the long axis approximately spanning solar elongation. The camera fields of view are aligned end-to-end and slightly overlapping such that they scan nearly the full sky each orbit about an orbital axis pointing at an equatorial declination of –8.8°. The individual 4 s data frames from each camera are stitched together to make a nearly full-sky map of each single orbit, excluding a $\sim 20°$ radius region around the Sun. Difference maps in either an Aitoff (Figure 1) or fisheye format [10] of the Thomson-scattered sunlight from density enhancements in the solar wind are corrected for scattered light and sky background to look for ICMEs as antisunward propagating features [13].

FIGURE 1. The camera 3, 2, 1 (blue, green, red) strips are merged into an Aitoff projection for each orbit. From [13].

BACKGROUND

The properties of the ICMEs observed by SMEI during the first 1.5 years of operations have been reported in [13]. The ICME leading edges have been tracked as far as possible through the SMEI field of view (FOV) to determine their speeds expressed in terms of elongation angle ε versus time. An example of a combined profile of a SMEI ICME and SOHO/LASCO [1] CME is shown in Figure 2. The elongation angle ε has been converted to a solar distance in AU using the assumed simple point-P approximation in which the height (AU) = sin ε. That approximation makes the dubious assumption of non-radial propagation for the leading edge and must be used with caution [11].

The tracking of the farthest point of the leading edge extracts only a small fraction of the ICME information available from the images. Of interest here

CP1216, *Twelfth International Solar Wind Conference*,
edited by M. Maksimovic, K. Issautier, N. Meyer-Vernet, M. Moncuquet, and F. Pantellini

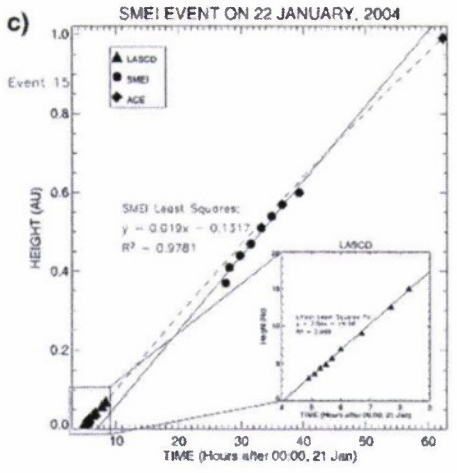

FIGURE 2. A plot of the leading edge of a SMEI ICME observed in 2004. The points in the lower left are from the SOHO/LASCO CME. Only a single point in PA is extracted from each LASCO and SMEI image for this plot. The goal of the current work is to examine the propagation of the broad front of the ICME rather than only at a single PA on the leading edge. From [9].

is to determine the 3-D propagation features of ICME structures. This can be accomplished by the combined STEREO/SECCHI [7] [4] and SOHO/LASCO instruments now in operation. In the meantime, we have an archival data base of SMEI images, many of which can be combined with LASCO images to study ICME propagation as a function of position angle (PA) in the sky. In principle these images can be used to look for non-radial expansions and speed variations from the ICME axis to its flanks. This is the goal of the present work.

Several studies motivated the current effort. Equatorward deflection of LASCO CME central PAs have been observed during periods of solar minimum [2] but not at maximum [3]. Coronal holes are known to deflect ICMEs near the Sun [6], so we have an opportunity to look for those effects at large radial distances. In addition, we can expect that interactions with solar wind streams can produce measurable distortions of the leading edge fronts.

The leading edge profiles of CMEs, particularly the most distant cases, may be density enhancements associated with shock fronts, piston fronts, or bright cores of the piston drivers. The line-of-sight locations of those leading edges are also open to some doubt. However, we suggest that there is much insight to be gained by determining not just the farthest points of the CME leading edges, but also the shapes of those leading edges and their variations with time and distance, which can reflect the effects of acceleration, magnetic restoring forces, and solar wind interactions.

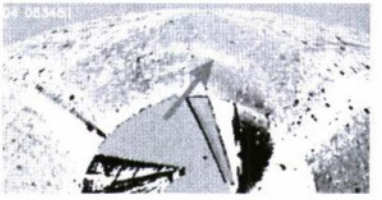

FIGURE 3. The arc of the 2004 July 21 ICME viewed in SMEI in an Aitoff format. The arrow points to the leading edge of the northern arc. The Sun center is indicated with the + sign and north is up.

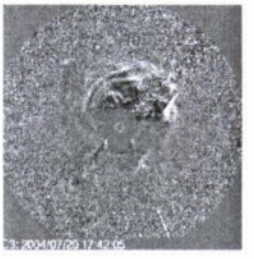

FIGURE 4. The earlier LASCO C3 image of the 2004 July 21 ICME. The C3 field of view is much smaller than the SMEI field of view, extending from 3.7 to 30 R$_\odot$, or about 7.5° from Sun center, here and in Figures 5 and 6.

SMEI DATA ANALYSIS

From an updated version of the SMEI ICME catalog [13] over the period 2003-2006 we selected the three ICMEs shown in Figures 3 through 6 to analyze the shapes of their leading edges. There were two bright arcs associated with the 2004 December 4 ICME, but we report details only on the broad SE arc. Each of the ICMEs was associated with a large LASCO CME. Large areas of the SMEI sky images degraded by backgrounds of geomagnetic particle radiation, auroral light, and the Moon are obvious in the SMEI images of Figures 3, 5, and 6.

We followed the analysis done for two ICMEs by Howard et al. (2007)[8], as shown schematically in Figure 7. The locations of the ICME leading edges were measured in sequences of images and were fitted to second order polynomials of the form

$$\varepsilon = \varepsilon_0 - \alpha\varepsilon_0(\mathrm{PA} - \mathrm{PA}_0)^2$$

where ε is the elongation and PA the position angle, both measured in degrees. The parameter α defines the curvature of the ICME front and is obtained from

$$d^2\varepsilon/d(\mathrm{PA})^2 = -2\alpha\varepsilon_0$$

We did least-squares best fits to the PA profiles to determine their curvatures α and centroids PA_0 as functions

TABLE 1. Parameters of the 2004 July 21 ICME

Date	Time UT	PA_0 (deg)	$10^5\alpha$ $(deg)^{-2}$	$\Delta\alpha/\alpha$	ε_0 (deg)
Jul 20	14:54	–25	5.51	0.290	C2
	17:42	–42	4.46	0.190	C3
Jul 21	13:52	CCV			
	15:38	CCV			
	17:24	CCV			
	20:51	–21	11.4	0.100	46
	22:31	CCV			
Jul 22	00:32	24	1.58	3.60	54
	01:55	18	3.46	0.440	59
	03:32	111	1.41	1.30	76
	05:12	CCV			
	06:52	CCV			
	08:34	CCV			
	10:21	287	0.401	1.40	

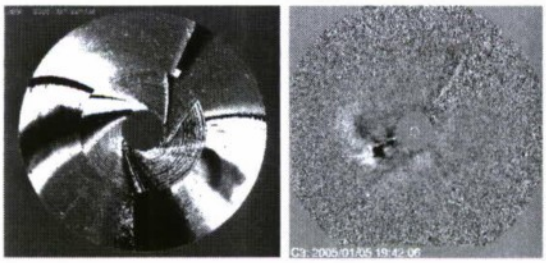

FIGURE 5. *Left*: The arc of the 2005 January 6 ICME viewed in SMEI in fisheye format. The arrow points to the leading edge of the southeastern arc. *Right*: The earlier LASCO C3 view of the 2005 January 6 ICME.

of time. The goal was to see how those parameters vary with increasing time and distance from the Sun. For each fit we determined α, ε_0, PA_0, and $\Delta\alpha/\alpha$, a measure of the uncertainty of α. We also included the LASCO C2 and C3 images, but without a distance scale. Typically we could measure 3 to 10 points of the leading edge on each SMEI subtracted image. The PA ranges of those points varied from image to image due to orbital changes of the degrading background features. Figure 8 shows the

TABLE 2. Parameters of the 2005 January 6 ICME

Date	Time UT	PA_0 (deg)	$10^5\alpha$ $(deg)^{-2}$	$\Delta\alpha/\alpha$	ε_0 (deg)
Jan 5	16:30	117	10.8	0.079	C2
	19:42	104	6.20	0.350	C3
Jan 6	14:52	85	10.6	0.770	31
	16:34	87	7.20	0.500	32
	18:14	77	6.00	0.550	35
	21:41	67	6.40	1.80	42
	23:20	CCV			

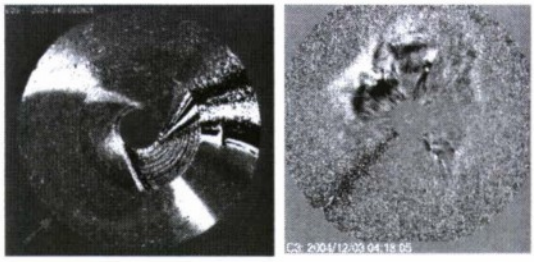

FIGURE 6. *Left*: The SE arc of the 2004 December 4 ICME viewed in SMEI in fisheye format. The arrow points to the leading edge of the broad arc in the SE. A second arc, observed in the NNW, was not analyzed. *Right*: The earlier LASCO C3 view of the 2004 December 3 CME.

TABLE 3. Parameters of the 2004 December 4 ICME

Date	Time UT	PA_0 (deg)	$10^5\alpha$ $(deg)^{-2}$	$\Delta\alpha/\alpha$	ε_0 (deg)
Dec 3	00:26	188	0.552	1.92	C2
	02:18	143	1.38	0.790	C3
Dec 5	02:20	97	4.29	0.148	96
	03:59	91	2.68	0.330	98
	05:38	86	2.47	0.430	104
	07:18	87	3.19	0.716	112
	08:58	Unc.			
	10:11	CCV			

results of a similar leading-edge analysis of a different SMEI ICME [8], with more extensive measurements than in our ICMEs. In that plot the distance $R = \tan \varepsilon$ for an assumed limb ICME.

Since the SMEI all-sky maps are mosaics of scans from each of the cameras, they are not single instantaneous images as are the LASCO images. The sky scans are made with a continuously decreasing PA, i.e., clockwise around the Sun, as viewed on the maps. Therefore the measured locations of an ICME leading edge as a function of PA in a single map will have significant differences in time that will produce some distortions to the leading-edge shape. The 360° sky scan takes 102 minutes, so a rough estimate of that timing difference is ~3.5°/minute. For the flanks of an ICME width of 60° or 90° this is about 17 or 26 minutes, respectively. The characteristic ICME elongation speed is ~1°/hour, so the elongation distortion across a 90° ICME span is < 1°, roughly the uncertainty in our measurements. Because the smaller PAs are measured later as the ICME propagates antisunward, a slight bias toward a smaller PA_0 is introduced in the measurements. Note that ICME leading-edge measurements made at various times at a fixed PA are not subject to this timing bias.

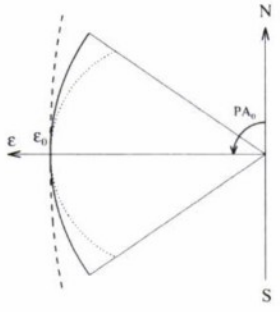

FIGURE 7. The leading edge data points ε versus PA are fitted to a parabola (dotted line). PA is measured from ecliptic north (N) and PA_0 indicates the centroid of the ICME. A fit with an $\alpha = 0$ corresponds to the solid-line circular front of $\varepsilon = \varepsilon_0$ as assumed in a conical model. An increasing positive α yields a more prolate shape, and a negative α yields a concave (CCV) front shown by the dashed line.

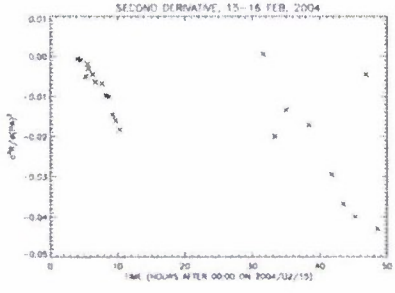

FIGURE 8. An example [8] showing the second rate of change of the distance R versus the PA, $d^2R/d(PA)^2$. The negative values reflect narrower curvature fits of the leading edges. The plots can also be exploited to determine deviations from radial propagation.

RESULTS

The parametric fits are given in Tables 1, 2, and 3 accompanying the event Figures. In some cases the fitting program found an outward concave parabolic fit (CCV in the tables and dashed curve of Figure 7) to be optimum for the data, which generally occurred when we could observe only a small segment of the ICME arc. The July 21 ICME of Figure 3 was the worst case in this regard. Even when expected convex fits were achieved, large changes in PA_0 and/or high values of $\Delta\alpha/\alpha$ indicated poor quality fits.

The leading-edge parabolic fits of the other two SMEI ICMEs were much better than that of July 21. For the January 6 (Figure 5) ICME PA_0 gradually decreased by rotating away from the ecliptic plane, with α approximately constant. The large SE arc of the 2004 December 4 (Figure 6) ICME was described by a slowly decreasing PA_0 near the ecliptic plane, with α again constant. The earlier LASCO CME of that event, however, was directed far south of the ecliptic plane.

The technique of fitting the broad fronts of ICMEs to parabolic fits should prove very useful for the STEREO observations. The SMEI database is substantial, but images with large, clear fields of view of distinct ICME fronts are few, and we have selected from the best events. This work should prove useful in interpreting both the physical structures and the locations of the ICMEs.

ACKNOWLEDGMENTS

SMEI is a collaborative project of the U. S. Air Force Research Laboratory, NASA, the University of California at San Diego, the University of Birmingham, U. K., Boston College, and Boston University. Financial support has been provided by the U. S. Air Force, the University of Birmingham, and NASA. The LASCO CME catalog is generated and maintained at the CDAW Data Center by NASA and The Catholic University of America in cooperation with the Naval Research Laboratory. SOHO is a project of international cooperation between ESA and NASA. We thank B. Ragot for Figure 7.

REFERENCES

1. G. E. Brueckner, R. A. Howard, et al., *Solar Phys.* **162**, 357-402 (1995).
2. H. Cremades and V. Bothmer, *Astron. Astrophys.* 422, 307-322 (2004).
3. H. Cremades, V. Bothmer, and D. Tripathi, *Adv. Space Res.* **38**, 461-465 (2006).
4. J. A. Davies, R. A. Harrison, et al., *Geophys. Res. Let.* **36**, L02102 (2009).
5. C. J. Eyles, G. M. Simnett et al., *Solar Phys.* **217**, 319-347 (2003).
6. N. Gopalswamy, P. Mäkelä et al., *J. Geophys. Res.* **114**, A00A22 (2009).
7. R. A. Howard, J. D. Moses et al., *Space Sci. Rev.* **136**, 67-115 (2008).
8. T. A. Howard, C. D. Fry, J. C. Johnston, and D. F. Webb, *Astrophys. J.* **667**, 610-625 (2007).
9. T. A. Howard, D. F. Webb, S. J. Tappin, D. R. Mizuno, and J. C. Johnston, *J. Geophys. Res.* **111**, A04105 (2006).
10. B. V. Jackson, A. Buffington, et al., *Solar Phys.* **225**, 177-207 (2004).
11. S. W. Kahler and D. F. Webb, *J. Geophys. Res.* **112**, A09103 (2007).
12. D. F. Webb, J. C. Johnston, R. R. Radick, and the SMEI Team, *EOS* **83**, 33,38-39 (2002).
13. D. F. Webb, D. R. Mizuno, et al., *J. Geophys. Res.* **111**, A12101 (2006).